Nonreciprocal superradiant quantum phase transition induced by magnon Kerr effect

Guo-Qiang Zhang,^{1,*} Si-Yan Lin,¹ Wei Feng,¹ Yi-Hao Kang,¹ and Wei Xiong^{2,3,†}

¹School of Physics, Hangzhou Normal University, Hangzhou, Zhejiang 311121, China

²Department of Physics, Wenzhou University, Zhejiang 325035, China

³International Quantum Academy, Shenzhen, 518048, China

(Dated: October 1, 2025)

Recently, proposals for realizing a nonreciprocal superradiant quantum phase transition (SQPT) have been put forward, based on either nonreciprocal interactions between two spin ensembles or the Sagnac-Fizeau shift in a spinning cavity. However, experimental implementation of such a nonreciprocal SQPT remains challenging. This motivates the search for new mechanisms capable of producing a nonreciprocal SQPT. Here, we propose an alternative approach to realize a nonreciprocal SQPT, induced by the magnon Kerr effect (MKE), in a cavity magnonic system, where magnons in a yttrium iron garnet (YIG) sphere are coupled to cavity photons. The Kerr coefficient K is positive (negative), i.e., K > 0 (K < 0), when the bias magnetic field is aligned along the crystallographic axis [100] ([110]) of the YIG sphere. We show that the steady-state phase diagrams differ significantly for both cases with K > 0 and K < 0, which is the origin of the nonreciprocal SQPT. By further studying the steady-state magnon occupation and its fluctuations versus the parametric drive strength, we demonstrate that the SQPT becomes nonreciprocal, characterized by distinct critical thresholds for K > 0 and K < 0. Moreover, we introduce a bidirectional contrast ratio to quantify this nonreciprocal behavior. Our work provides a new mechanism for realizing the nonreciprocal SQPT, with potential applications in designing nonreciprocal quantum devices.

I. INTRODUCTION

Superradiant quantum phase transition (SOPT) in the Dicke model was first predicted by Hepp et al. in 1973 [1, 2]. The Dicke model describes the collective coupling of N twolevel atoms to a quantized light field [3]. In the thermodynamic limit with the number of atoms $N \to +\infty$, the system undergoes a SQPT from the normal phase to the superradiant phase at zero temperature as the coupling strength exceeds a critical value [4, 5]. Below the critical coupling, the system is in the normal phase, where the atoms remain in their ground state and the cavity field is in the vacuum state. Above the critical coupling, the system enters the superradiant phase, characterized by collective excitations of both the atomic ensemble and the cavity field. With advances in experimental capabilities, the SQPT in the Dicke model and its variants (e.g., Tavis-Cummings model [6, 7], Rabi model [8, 9], Jaynes-Cummings model [10, 11], and coupled multi-oscillator model [12–14]) has been observed in a variety of quantum platforms. These include Bose-Einstein condensates within optical cavities [15–18], degenerate Fermi gases inside an optical cavity [19, 20], circuit QED systems [21-23], trapped ions [24, 25], nuclear-magnetic-resonance systems [26, 27], and so on.

Recently, Fruchart *et al.* established a general theory of nonreciprocal phase transitions, showing that time-dependent phases arise from asymmetric interactions among multiple species or fields [28]. The nonreciprocal phenomenon refers to that the system responds differently when an external field is applied in opposite directions. Due to potential applications in quantum technologies, various nonreciprocal quantum effects have been studied, such as thermal noise routers [29],

nonreciprocal photon blockade [30], one-way quantum amplifiers [31–33], and nonreciprocal magnon blockade [34]. Following the framework of Ref. [28], the nonreciprocal SQPT was proposed in a nonreciprocal Dicke model, with quantum-light-mediated nonreciprocal interactions between two spin ensembles [35]. Separately, two groups have independently proposed realizing a nonreciprocal SQPT by exploiting the Sagnac-Fizeau shift in a spinning cavity [36, 37]. However, the key elements of these proposals-specifically, the required nonreciprocal interactions between two spin ensembles [35] and the Sagnac-Fizeau shift in a spinning resonator [36, 37]-present major challenges for existing experimental quantum platforms that have demonstrated the SQPT [15–27]. It is therefore imperative to explore new theoretical mechanisms for realizing a nonreciprocal SOPT.

Owing to their excellent tunability and design flexibility, cavity magnonic systems have emerged as well-suited platforms for exploring novel physical phenomena [38–48]. In Ref. [49], frequency shifts of both the magnon and cavity modes induced by the magnon Kerr effect (MKE) were experimentally observed by directly driving a yttrium iron garnet (YIG) sphere within a microwave cavity. The MKE, which originates from magnetocrystalline anisotropy in YIG, describes magnon-magnon interactions. It can lead to multistability of cavity magnon polaritons [50–55], magnon-photon entanglement [56, 57], long-distance spin-spin coupling [58], and unidirectional microwave transmission [59-61], among other effects. A notable feature of the MKE is that the Kerr coefficient depends on the direction of the bias magnetic field applied to the YIG sphere: the Kerr coefficient is positive when the field is aligned with the crystallographic axis [100], and negative when aligned with the axis [110] [50, 51]. It is this directional dependence that makes cavity magnonic systems a promising platform for studying nonreciprocal quantum effects, such as nonreciprocal entanglement [62-65], nonreciprocal steering [66], nonreciprocal magnon blockade [67], and

^{*} zhangguoqiang@hznu.edu.cn

[†] xiongweiphys@wzu.edu.cn

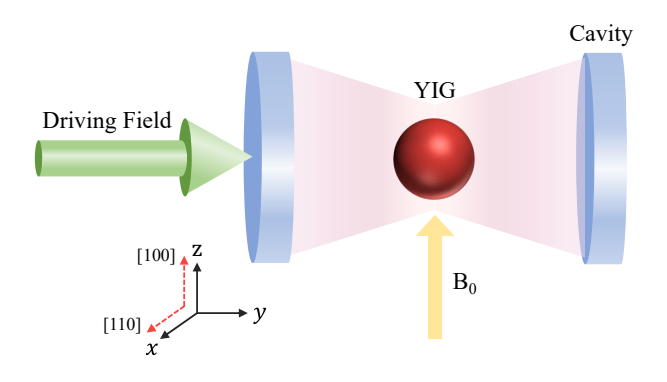


FIG. 1. Schematic diagram of the proposed cavity magnonic system. The system comprises a parametrically driven microwave cavity and a YIG sphere magnetized to saturation by a bias magnetic field B_0 . The magnetic field is aligned along either the crystallographic axis [100] or [110] (see the red-arrowed lines) of the YIG sphere.

nonreciprocal mechanical squeezing [68].

In this work, we propose a scheme for realizing a nonreciprocal SQPT induced by MKE in a cavity magnonic system. The system consists of a magnon mode in a YIG sphere coupled to a cavity mode via the magnetic-dipole interaction, where the cavity is subject to a parametric drive, and the magnon mode exhibits the MKE. By analyzing the stability of the solutions for the magnon occupation, we obtain the steady-state phase diagram, which comprises three distinct phases: normal phase, superradiant phase and bistable phase. The phase diagram differs significantly when the bias magnetic field is aligned along the [100] or [110] crystallographic axis of the YIG sphere, corresponding to a positive (K > 0)or negative (K < 0) Kerr coefficient, respectively [50, 51]. We further examine the steady-state magnon number and its fluctuations as functions of the parametric drive strength, revealing that the SQPT becomes nonreciprocal, with different critical thresholds for K > 0 and K < 0. To quantify this behavior, we introduce a bidirectional contrast ratio that characterizes the degree of nonreciprocity in the SQPT. Our work provides an alternative approach for realizing a nonreciprocal SQPT [35–37] and offers useful guidance for the experimental realization of this phenomenon in the future.

The remainder of this paper is structured as follows. In Sec. II, we introduce the proposed cavity magnonic system and derive the steady-state solutions for the magnon occupation. Section III presents the steady-state phase diagram based on a stability analysis of these solutions, followed by a detailed investigation of the MKE-induced nonreciprocal SQPT. Finally, a brief summary is given in Sec. IV.

II. MODEL

As depicted in Fig. 1, the considered cavity magnonic system consists of a microwave cavity and a millimeter-sized YIG sphere, where the cavity is pumped by a parametric drive, and the YIG sphere is magnetized to saturation by a bias static magnetic field. The YIG sphere supports a Kit-

TABLE I. The parameter conditions (PCs) for $|M|_{\pm}^2 > 0$ in both cases of K > 0 and K < 0, where the solution $|M|^2 = |M|_{-}^2 (|M|^2 = |M|_{+}^2)$ is unstable for all parameter values in the case of K > 0 (K < 0) and not considered here.

nonnegativity constraint	PCs for $K > 0$	PCs for $K < 0$
$ M _+^2 > 0$	$\Omega > \Omega_1 \text{ for } \Delta_m/\Delta_a < \xi \text{ or } \Omega > \Omega_2 \text{ for } \Delta_m/\Delta_a > \xi$	trivial solution
$ M ^2 > 0$	trivial solution	$\Omega > \Omega_2 \text{ for } \Delta_m/\Delta_a < \xi \text{ or } \Omega > \Omega_1 \text{ for } \Delta_m/\Delta_a > \xi$

tle mode (with frequency ω_m), which is coupled to the cavity mode (with frequency ω_a) via the collective magnetic-dipole interaction. Taking into account both the system's dissipation and the interaction among magnons (i.e., MKE), the parametrically driven cavity magnonic system can be described by the following effective non-Hermitian Hamiltonian (see Appendix A):

$$H_{\text{eff}} = (\Delta_a - i\kappa_a)a^{\dagger}a + (\Delta_m - i\gamma_m)m^{\dagger}m + \frac{K}{2}m^{\dagger}m^{\dagger}mm + g_m(a^{\dagger}m + am^{\dagger}) + \frac{\Omega}{2}(a^{\dagger}a^{\dagger} + aa), \tag{1}$$

where a^{\dagger} and a (m^{\dagger} and m) are the creation and annihilation operators of the cavity mode (magnon mode), $\Delta_{a(m)} =$ $\omega_{a(m)} - \omega_d/2$ (> 0) is the frequency detuning of the cavity mode (magnon mode) from the drive field, κ_a (γ_m) is the decay rate of the cavity mode (magnon mode), K is the Kerr coefficient, g_m is the coupling strength between cavity mode and magnon mode, and $\omega_d(\Omega)$ is the frequency (strength) of parametric drive. Here the MKE results from the magnetocrystalline anisotropy of the YIG sphere, and the sign of Kerr coefficient K can be controlled via adjusting the direction of the bias magnetic field [50, 51]. When the bias magnetic field is aligned along the crystallographic axis [100], the Kerr coefficient K is positive (K > 0). In contrast, K becomes negative (K < 0) for aligning the bias magnetic field along the crystallographic axis [110]. The dependence of K on the direction of the bias magnetic field is the origin of the nonreciprocal SQPT (cf. Sec. III). The effective Hamiltonian H_{eff} maintains invariance under the transformation $a \rightarrow -a$ and $b \rightarrow -b$, demonstrating parity symmetry [4, 5]. Defining the parity operator $\prod = \exp[i\pi(a^{\dagger}a + b^{\dagger}b)]$, this symmetry can be expressed as the commutation relation $[H_{\text{eff}}, \prod] = 0$. In our system, the spontaneous breaking of parity symmetry occurs when the cavity magnonic system undergoes a phase transition from the normal phase to superradiant phase.

The dynamics of the cavity magnonic system can be described through the following quantum Langevin equations [69]:

$$\dot{a} = -i(\Delta_a - i\kappa_a)a - ig_m m - i\Omega a^{\dagger} + \sqrt{2\kappa_a} a_{\rm in},$$

$$\dot{m} = -i(\Delta_m - i\gamma_m)m - iKm^{\dagger} mm - ig_m a + \sqrt{2\gamma_m} m_{\rm in}, (2)$$

where $o_{\rm in}$ is the input noise operator for the mode o (o=a,m), satisfying $\langle o_{\rm in} \rangle = 0$. Under the Markovian approximation, the noise operator $o_{\rm in}$ is characterized by the following two-time correlation functions: $\langle o_{\rm in}(t)o_{\rm in}^{\dagger}(t')\rangle = [\overline{n}_o(\omega_o)+1]\delta(t-t')$ and $\langle o_{\rm in}^{\dagger}(t)o_{\rm in}(t')\rangle = \overline{n}_o(\omega_o)\delta(t-t')$ with $\overline{n}_o(\omega_o) = [\exp(\hbar\omega_o/k_BT)-t]$

1]⁻¹ denoting the equilibrium mean thermal excitation number of the mode o, where k_B is the Boltzmann constant and T is the bath temperature. To analyze the steady-state behavior of the cavity magnonic system, we perform a linearization of Eq. (2) by decomposing the operators as $a = A + \delta a$ and $m = M + \delta m$, where A(M) represents the expectation value of operator a(m), and $\delta a(\delta m)$ denotes the quantum fluctuation with $\langle \delta a \rangle = \langle \delta m \rangle = 0$. Following from Eq. (2), the expectation values A and M satisfy

$$\dot{A} = -i(\Delta_a - i\kappa_a)A - ig_m M - i\Omega A^*,$$

$$\dot{M} = -i(\Delta_m + K|M|^2 - i\gamma_m)M - ig_m A,$$
(3)

and the fluctuation operators δa and δm obey

$$\delta \dot{a} = -i(\Delta_a - i\kappa_a)\delta a - ig_m\delta m - i\Omega\delta a^{\dagger} + \sqrt{2\kappa_a}a_{\rm in},$$

$$\delta \dot{m} = -i(\widetilde{\Delta}_m - i\gamma_m)\delta m - ig_m\delta a - iF\delta m^{\dagger} + \sqrt{2\gamma_m}m_{\rm in}, (4)$$

where $\widetilde{\Delta}_m = \Delta_m + 2K|M|^2$ and $F = KM^2$. For obtaining the linear fluctuation equation (4), all small high-order fluctuation terms have been neglected. The steady-state solutions for $|M|^2$ and $|A|^2$, obtained from Eq. (3) with $\dot{A} = \dot{M} = 0$, exhibit three branches due to the MKE:

$$|M|_0^2 = 0$$
, $|M|_{\pm}^2 = \left(-\Delta_m' \pm \sqrt{\eta^2 G^2 - {\gamma_m'}^2}\right)/K$, (5)

and

$$|A|_0^2 = 0$$
, $|A|_{\pm}^2 = \left[\left(\Delta_m + K |M|_{\pm}^2 \right)^2 + \gamma_m^2 \right] |M|_{\pm}^2 / g_m^2$, (6)

where $\Delta'_m = \Delta_m - \eta \Delta_a$, $\gamma'_m = \gamma_m + \eta \kappa_a$ and $\eta = g_m^2/(\Delta_a^2 + \kappa_a^2 - \Omega^2)$. Obviously, the photon number $|A|^2$ is dependent on the magnon number $|M|^2$.

In this study, we choose the magnon number $|M|^2$ as the order parameter for the SQPT. The nonnegativity constraint on the magnon number $|M|^2$ restricts the valid solutions to $|M|_{\pm}^2 \geq 0$. Table I summarizes the conditions for $|M|_{+}^2 > 0$ when K > 0 and $|M|_{-}^2 > 0$ when K < 0, where we exclude the trivial solutions $|M|_{-}^2$ when K > 0 and $|M|_{+}^2$ when K < 0 due to their instability across all parameters (see Fig. 2 and related discussions). For K > 0, the constraint $|M|_{+}^2 > 0$ requires $\Omega > \Omega_1$ when $\Delta_m/\Delta_a < \xi$ or $\Omega > \Omega_2$ for $\Delta_m/\Delta_a > \xi$, with the critical ratio ξ defined as

$$\xi = \frac{2\gamma_m^2}{\sqrt{4(\Delta_a^2 + \kappa_a^2)\gamma_m^2 + (4\kappa_a\gamma_m + g_m^2)g_m^2 - (2\kappa_a\gamma_m + g_m^2)}}.$$
 (7)

The critical drive strengths Ω_1 and Ω_2 are respectively given by

$$\Omega_1 = \sqrt{\Delta_a^2 + \kappa_a^2 + (4\kappa_a \gamma_m + g_m^2)g_m^2/4\gamma_m^2} - g_m^2/2\gamma_m,$$
 (8)

and

$$\Omega_2 = \sqrt{\Delta_a^2 + \kappa_a^2 - (2\Delta_a \Delta_m - 2\kappa_a \gamma_m - g_m^2)g_m^2/(\Delta_m^2 + \gamma_m^2)}, \quad (9)$$

which determined the boundaries between different phases in the steady-state phase diagram of the cavity magnonic system (see Fig. 2). In particular, $\Omega_1 = \Omega_2$ at $\Delta_m/\Delta_a = \xi$. For K < 0, the constraint $|M|_-^2 > 0$ is satisfied when $\Omega > \Omega_2$ for $\Delta_m/\Delta_a < \xi$ or $\Omega > \Omega_1$ for $\Delta_m/\Delta_a > \xi$.

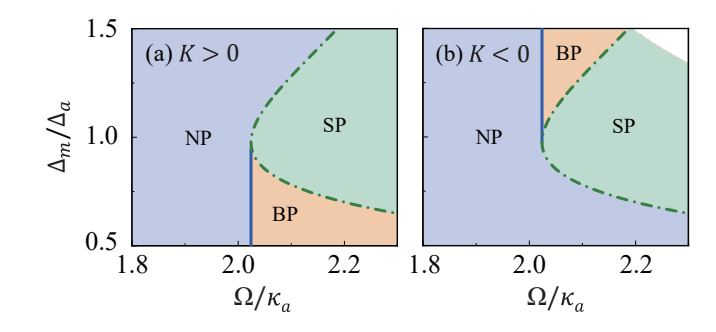


FIG. 2. Steady-state phase diagram of the cavity magnonic system versus the normalized drive strength Ω/κ_a and the detuning ratio Δ_m/Δ_a , where (a) K>0 and (b) K<0. NP, SP, and BP represent the normal phase, superradiant phase, and bistable phase, respectively. The white background in the upper-right corner of panel (b) indicates the unstable region. The vertical blue solid line marks the critical drive strength $\Omega=\Omega_1$, while the green dashed-dotted curve indicates the critical drive strength $\Omega=\Omega_2$. Other parameters are chosen to be $\Delta_a/\kappa_a=3$, $g_m/\kappa_a=2.4$, and $\gamma_m/\kappa_a=1$.

TABLE II. Stable solutions (SSs) in each phase for both cases of K > 0 and K < 0.

phase type	SSs for $K > 0$	SSs for $K < 0$
normal phase	$ M ^2 = 0$	$ M ^2 = 0$
superradiant phase	$ M ^2 = M _+^2$	$ M ^2 = M ^2$
bistable phase	$ M ^2 = 0$ and $ M ^2 = M _+^2$	$ M ^2 = 0$ and $ M ^2 = M ^2$

III. NONRECIPROCAL SUPERRADIANT QUANTUM PHASE TRANSITION

For examining the stability of the solutions for $|M|^2$ in Eq. (5), we need to investigate the fluctuations of the system. By introducing the quadrature operators $x_a = (\delta a^{\dagger} + \delta a)/\sqrt{2}$, $y_a = i(\delta a^{\dagger} - \delta a)/\sqrt{2}$, $x_m = (\delta m^{\dagger} + \delta m)/\sqrt{2}$, and $y_m = i(\delta m^{\dagger} - \delta m)/\sqrt{2}$, we recast Eq. (4) and its complex conjugate expression into the compact matrix form:

$$\dot{u}(t) = \Lambda u(t) + f_{\rm in}(t), \tag{10}$$

where $u(t) = [x_a(t), y_a(t), x_m(t), y_m(t)]^T$ represents the vector of quadrature components, $f_{\rm in}(t) = [\sqrt{2\kappa_a} \, x_a^{\rm (in)}, \sqrt{2\kappa_a} \, y_a^{\rm (in)}, \sqrt{2\gamma_m} \, x_m^{\rm (in)}, \sqrt{2\gamma_m} \, y_m^{\rm (in)}]^T$ denotes the vector of noise quadratures, defined as $x_a^{\rm (in)} = (a_{\rm in}^\dagger + a_{\rm in})/\sqrt{2},$ $y_a^{\rm (in)} = i(a_{\rm in}^\dagger - a_{\rm in})/\sqrt{2}, x_m^{\rm (in)} = (m_{\rm in}^\dagger + m_{\rm in})/\sqrt{2},$ and $y_m^{\rm (in)} = i(m_{\rm in}^\dagger - m_{\rm in})/\sqrt{2},$ and the drift matrix Λ is given by

$$\mathbf{\Lambda} = \begin{pmatrix} -\kappa_a & \Delta_a - \Omega & 0 & g_m \\ -\Delta_a - \Omega & -\kappa_a & -g_m & 0 \\ 0 & g_m & -\gamma_m + \operatorname{Im}[F] & \widetilde{\Delta}_m - \operatorname{Re}[F] \\ -g_m & 0 & -\widetilde{\Delta}_m - \operatorname{Re}[F] & -\gamma_m - \operatorname{Im}[F] \end{pmatrix}.$$
(11)

The stability of solutions $|M|_0^2$ and $|M|_{\pm}^2$ is governed by the spectral properties of the corresponding drift matrix Λ [70]. A given solution is stable only if all eigenvalues λ_k of matrix Λ satisfy $\text{Re}(\lambda_k) < 0$ for k = 1, 2, 3, 4; otherwise, it is unstable.

Based on the stability analysis of the solutions in Eq. (5), we plot the steady-state phase diagram of the system as a function of the normalized drive strength Ω/κ_a and the detuning

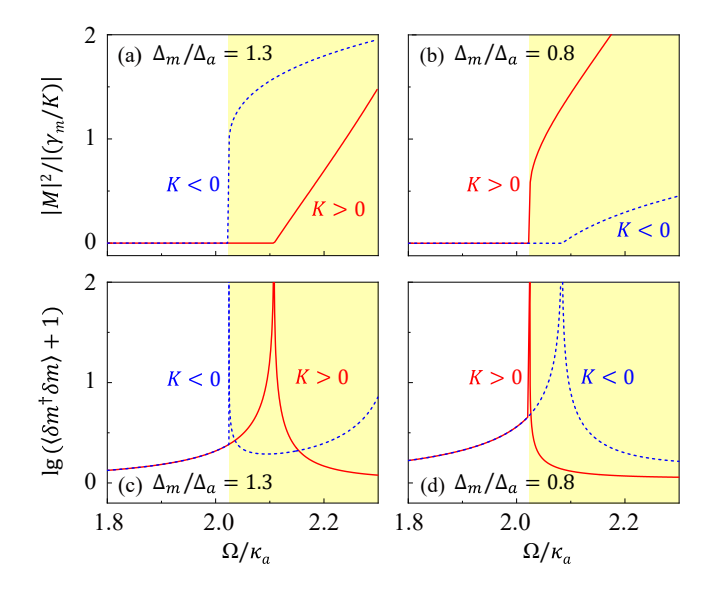


FIG. 3. (a),(b) Scaled steady-state magnon numbers $|M|^2/|(\gamma_m/K)|$ and (c),(d) magnon number fluctuations $\lg(\langle \delta m^\dagger \delta m \rangle + 1)$ versus the normalized drive strength Ω/κ_a , where T=0. Yellow shaded regions mark the nonreciprocal domains of SQPT, where $|M|^2(K>0) \neq |M|^2(K<0)$. The red solid curves correspond to K>0, and the blue dashed curves correspond to K<0. The detuning ratios are $\Delta_m/\Delta_a=1.3$ and $\Delta_m/\Delta_a=0.8$ in panels (a),(c) and (b),(d), respectively. Other parameters are the same as those in Fig. 2.

ratio Δ_m/Δ_a in Fig. 2. Note that the white background in the upper-right corner of Fig. 2(b) indicates the unstable regime, where all three solutions for $|M|^2$ are unstable. Figures 2(a) and 2(b) correspond to K > 0 and K < 0, respectively, which can be realized by aligning the bias magnetic field parallel to the [100] and [110] crystallographic axes of the YIG sphere [50, 51]. The difference between these two panels demonstrates the nonreciprocity of the SQPT. The phase diagrams exhibits three distinct phases: normal phase (light blue area), superradiant phase (light green area) and bistable phase (light orange area), where the boundaries among them are determined by the vertical blue solid line $[\Omega = \Omega_1]$ given in Eq. (8)] and the blue dash-dotted curve $[\Omega = \Omega_2]$ given in Eq. (9)]. Table II summarizes the stable solutions in each phase. In the normal phase, the solution $|M|^2 = 0$ is stable for both K > 0 and K < 0, corresponding to the vacuum state. In the superradiant phase, the solution $|M|^2 = |M|_{\perp}^2$ for K > 0 ($|M|^2 = |M|_-^2$ for K < 0) becomes stable, and the system exhibits macroscopic magnon excitations. In the bistable phase, both $|M|^2 = 0$ and $|M|^2 = |M|_+^2$ for K > 0 ($|M|^2 = 0$ and $|M|^2 = |M|_-^2$ for K < 0) are stable, and the system's initial state determines whether macroscopic magnon excitations occur [12]. For the parameters used in Fig. 2, the critical ratio ξ from Eq. (7) is $\xi = 0.976$. When $\Delta_m/\Delta_a < \xi$, the boundary between normal phase and bistable phase (normal phase and superradiant phase) is given by $\Omega = \Omega_1$ ($\Omega = \Omega_2$) for K > 0 (K < 0). Conversely, when $\Delta_m/\Delta_a > \xi$, the boundary between normal phase and superradiant phase (normal phase and bistable phase) is given by $\Omega = \Omega_2$ ($\Omega = \Omega_1$) for K > 0(K < 0). Regardless of the value of Δ_m/Δ_a and the sign of K,

the curve $\Omega = \Omega_2$ universally defines the boundary between bistable phase and superradiant phase.

In Figs. 3(a), we displays the scaled steady-state magnon number $|M|^2/|(\gamma_m/K)|$ as a function of the normalized drive strength Ω/κ_a for a fixed detuning ratio $\Delta_m/\Delta_a = 1.3$ (> ξ = 0.976). Yellow shaded regions indicate the nonreciprocal domains of SQPT, where $|M|^2(K > 0) \neq |M|^2(K < 0)$. In the case of K < 0, the magnon number exhibits a discontinuous jump from zero to a finite value at the critical point $\Omega/\kappa_a = 2.025$ as the normalized drive strength Ω/κ_a increases across this threshold (blue dashed curve), signifying a second-order SQPT from the normal phase to the superradiant phase. However, for K > 0, the transition becomes first-order (i.e., a continuous SQPT), and the critical point shifts to $\Omega/\kappa_a = 2.108$ (red solid curve). Figure 3(b) shows $|M|^2/|(\gamma_m/K)|$ versus Ω/κ_a by taking $\Delta_m/\Delta_a = 0.8$ ($<\xi=0.976$), where nonreciprocal SQPT is also evident. Unlike the case with $\Delta_m/\Delta_a > \xi$ [cf. Figs. 3(a) and 3(b)], the system now undergoes a second-order SQPT from the normal phase to the superradiant phase at $\Omega/\kappa_a = 2.084$ for K < 0(blue dashed curve), while the transition remains first-order at $\Omega/\kappa_a = 2.025$ if K > 0 (red solid curve).

In order to quantitatively characterize the nonreciprocity in the SQPT, we introduce the bidirectional contrast ratio:

$$I = \begin{cases} 0, & |M|^2(K > 0) = |M|^2(K < 0), \\ \left| \frac{|M|^2(K > 0) - |M|^2(K < 0)}{|M|^2(K > 0) + |M|^2(K < 0)} \right|, & |M|^2(K > 0) \neq |M|^2(K < 0), \end{cases}$$
(12)

which satisfies $0 \le I \le 1$. This parameter quantifies the degree of nonreciprocity in the SQPT: a nonzero I signals the emergence of nonreciprocal behavior. The minimum value $I_{\min} = 0$ corresponds to a reciprocal SQPT, while the maximum value $I_{\text{max}} = 1$ represents an ideal nonreciprocal SQPT. In Fig. 4, we show the bidirectional contrast ratio \mathcal{I} as a function of the normalized drive strength Ω/κ_a and the detuning ratio Δ_m/Δ_a . The white region in the upper-right corner corresponds to the unstable regime identified in Fig. 2(b). The vertical blue solid line (red dashed-dotted curve) marks the critical drive strength $\Omega = \Omega_1 = 2.025$ ($\Omega = \Omega_2$). The bidirectional contrast ratio I attains its minimum value $I_{min} = 0$ in the black region ($\Omega < \Omega_1$), where the system remains in the normal phase for both K > 0 and K < 0, indicating reciprocal SQPT. Notably, two red regions appear for $\Omega_1 < \Omega < \Omega_2$, where *I* reaches its maximum value $I_{\text{max}} = 1$, corresponding to an ideal nonreciprocal SQPT. In the lower (upper) red region, the system is in the superradiant phase (normal phase) for K > 0 but remains in the normal phase (superradiant phase) for K < 0. In the remaining region $(\Omega > \Omega_2)$, the bidirectional contrast ratio lies between 0 and 1 (i.e., 0 < I < 1). Here, the system is in the superradiant phase for both K > 0 and K < 0, but the order parameters differ: $|M|^2(K > 0) = |M|_+^2 \neq |M|^2(K < 0) = |M|_-^2$

To show more characteristics of the nonreciprocal SQPT, we examine the magnon number fluctuations $\langle \delta m^{\dagger} \delta m \rangle$ on top of the stable mean-field solutions for $|M|^2$. The quantum fluctuations of the cavity magnonic system are described by a 4×4 covariance matrix $\mathcal{V}(t)$, with elements defined as $\mathcal{V}_{ij}(t)$ =

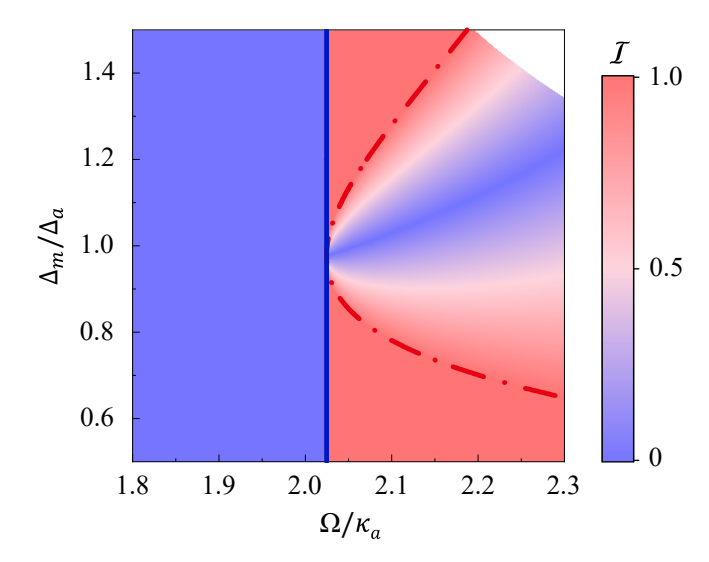


FIG. 4. Bidirectional contrast ratio I as a function of the normalized drive strength Ω/κ_a and the detuning ratio Δ_m/Δ_a . The white background in the upper-right corner corresponds to the unstable region in Fig. 2(b). The vertical blue solid line marks the critical drive $\Omega = \Omega_1$, and the red dashed-dotted curve indicates $\Omega = \Omega_2$. Other parameters are the same as those in Fig. 2.

 $\langle u_i(t)u_j(t')+u_j(t')u_i(t)\rangle/2$ (i, j=1, 2, 3, 4). In our model, the magnon number fluctuations $\langle \delta m^{\dagger} \delta m \rangle = [(V_{33} + V_{44}) - 1]/2$ are related to the diagonal elements of the steady-state covariance matrix $\mathcal{V}(+\infty)$ [71], which can be straightforwardly obtained by solving the so-called Lyapunov equation

$$\Lambda \mathcal{V} + \mathcal{V} \Lambda^T = -\mathcal{D}, \tag{13}$$

where the diffusion matrix \mathcal{D} , determined by $\mathcal{D}_{ij}\delta(t-t') = \langle f_{in,i}(t)f_{in,j}(t') + f_{in,j}(t')f_{in,i}(t)\rangle/2$, takes the form $\mathcal{D} = \mathrm{diag}\left[(2\bar{n}_a+1)\kappa_a,(2\bar{n}_a+1)\kappa_a,(2\bar{n}_m+1)\gamma_m,(2\bar{n}_m+1)\gamma_m\right]$. For the nonreciprocal behavior of the SQPT shown in Figs. 3(a) and 3(b), the corresponding magnon number fluctuations are presented in Figs. 3(c) and 3(d), respectively. For clarity, we plot $\lg(\langle \delta m^\dagger \delta m \rangle + 1)$ as a function of the normalized drive strength Ω/κ_a . Here, the red solid curves correspond to K>0, and the blue dashed curves to K<0. The magnon number fluctuations exhibit clear nonreciprocity, consistent with the nonreciprocal behavior of SQPT. In all cases, the fluctuations diverge near the critical point of the SQPT but approach zero far from the critical point [cf. Figs. 3(a) and 3(b)].

IV. CONCLUSION

In summary, we have demonstrated that the MKE in a cavity magnonic system offers a viable pathway to achieve a nonreciprocal SQPT [35–37]. The proposed setup, comprising a YIG sphere coupled to a microwave cavity, exhibits markedly different phase diagrams under positive and negative Kerr coefficients-controlled by orienting the bias magnetic field along different crystallographic axes of the YG sphere [50, 51]. These distinct phase boundaries directly lead

to nonreciprocal critical behavior, as confirmed by analyzing the magnon occupation and its fluctuations around the transition. The introduction of a bidirectional contrast ratio further allows quantitative characterization of the nonreciprocity. Our results establish cavity magnonics as a promising platform for exploring nonreciprocal SQPT and may inform future designs of quantum devices requiring directional control.

ACKNOWLEDGMENTS

This work is supported by the National Natural Science Foundation of China (Grants No. 12205069 and No. 12204139), the National Key Research and Development Program of China (Grant No. 2024YFA1408900), the Natural Science Foundation of Zhejiang Province (Grant No. LY24A040004), Zhejiang Province Key R&D Program of China (Grant No. 2025C01028), and Shenzhen International Quantum Academy (Grant No. SIQA2024KFKT010).

Appendix A: Derivation of the effective non-Hermitian Hamiltonian in Eq. (1)

As shown in Fig. 1, the magnon mode in the YIG sphere is coupled to the cavity mode. Including both the parametric drive and the MKE, the total Hamiltonian of the system is given by

$$H = \omega_a a^{\dagger} a + \omega_m m^{\dagger} m + \frac{K}{2} m^{\dagger} m^{\dagger} m m + g_m (a^{\dagger} m + a m^{\dagger}) + \frac{\Omega}{2} (a^{\dagger} a^{\dagger} e^{-i\omega_d t} + a a e^{i\omega_d t}), \tag{A1}$$

where a^{\dagger} and m^{\dagger} (a and m) are the creation (annihilation) operators for the cavity and magnon modes with frequencies ω_a and ω_m , respectively, K is the Kerr coefficient, g_m is the coupling strength between cavity and magnon modes, and Ω (ω_d) is the strength (frequency) of parametric drive. In the rotating frame at $\omega_d/2$, the Hamiltonian in Eq. (A1) becomes

$$H = \Delta_a a^{\dagger} a + \Delta_m m^{\dagger} m + \frac{K}{2} m^{\dagger} m^{\dagger} m m + g_m (a^{\dagger} m + a m^{\dagger}) + \frac{\Omega}{2} (a^{\dagger} a^{\dagger} + a a), \tag{A2}$$

where $\Delta_a = \omega_a - \omega_d/2$ and $\Delta_m = \omega_m - \omega_d/2$ represent the detunings of the cavity and magnon modes from the parametric drive, respectively. With the Heisenberg-Langevin approach [69], the quantum dynamics of the system is governed by

$$\dot{a} = -i(\Delta_a - i\kappa_a)a - ig_m m - i\Omega a^{\dagger} + \sqrt{2\kappa_a} a_{\rm in},$$

$$\dot{m} = -i(\Delta_m - i\gamma_m)m - iKm^{\dagger}mm - ig_m a + \sqrt{2\gamma_m} m_{\rm in}, (A3)$$

which is Eq. (2) in the main text. Here, κ_a (γ_m) denotes the decay rate of the cavity mode (magnon mode), and $a_{\rm in}$ ($m_{\rm in}$) is the corresponding input noise operator. Rewriting Eq. (A3) in

the form

$$\dot{a} = -i[a, H_{\text{eff}}] + \sqrt{2\kappa_a} a_{\text{in}},$$

$$\dot{m} = -i[m, H_{\text{eff}}] + \sqrt{2\gamma_m} m_{\text{in}},$$
(A4)

yields the effective non-Hermitian Hamiltonian H_{eff} presented in Eq. (1).

- [1] K. Hepp and E. H. Lieb, On the superradiant phase transition for molecules in a quantized radiation field: The Dicke maser model, Ann. Phys. **76**, 360 (1973).
- [2] Y. K. Wang and F. T. Hioe, Phase transition in the dicke model of superradiance, Phys. Rev. A 7, 831 (1973).
- [3] R. H. Dicke, Coherence in spontaneous radiation processes, Phys. Rev. **93**, 99 (1954).
- [4] C. Emary and T. Brandes, Quantum Chaos Triggered by Precursors of a Quantum Phase Transition: The Dicke Model, Phys. Rev. Lett. 90, 044101 (2003).
- [5] C. Emary and T. Brandes, Chaos and the quantum phase transition in the Dicke model, Phys. Rev. E 67, 066203 (2003).
- [6] O. Castaños, R. López-Peña, E. Nahmad-Achar, J. G. Hirsch, E. López-Moreno, and J. E. Vitela, Coherent state description of the ground state in the Tavis-Cummings model and its quantum phase transitions, Phys. Scr. 79, 065405 (2009).
- [7] J. H. Zou, T. Liu, M. Feng, W. L. Yang, C. Y. Chen, and J. Twamley, Quantum phase transition in a driven Tavis-Cummings model, New J. Phys. 15, 123032 (2013).
- [8] S. Ashhab, Superradiance transition in a system with a single qubit and a single oscillator, Phys. Rev. A **87**, 013826 (2013).
- [9] M. J. Hwang, R. Puebla, and M. B. Plenio, Quantum Phase Transition and Universal Dynamics in the Rabi Model, Phys. Rev. Lett. 115, 180404 (2015).
- [10] M. J. Hwang and M. B. Plenio, Quantum Phase Transition in the Finite Jaynes-Cummings Lattice Systems, Phys. Rev. Lett. 117, 123602 (2016).
- [11] C. Liu, and J. F. Huang, Quantum phase transition of the Jaynes-Cummings model, Sci. China-Phys. Mech. Astron. 67, 210311 (2024).
- [12] G. Q. Zhang, Z. Chen, W. Xiong, C. H. Lam, and J. Q. You, Parity-symmetry-breaking quantum phase transition via parametric drive in a cavity magnonic system, Phys. Rev. B 104, 064423 (2021).
- [13] Y. Qin, S. C. Li, K. Li, and J. J. Song, Controllable quantum phase transition in a double-cavity magnonic system, Phys. Rev. B 106, 054419 (2022)
- [14] B. Wang, F. Nori, and Z. L. Xiang, Quantum Phase Transitions in Optomechanical Systems, Phys. Rev. Lett. 132, 053601 (2024).
- [15] K. Baumann, C. Guerlin, F. Brennecke, and T. Esslinger, Dicke quantum phase transition with a superfluid gas in an optical cavity, Nature 464, 1301 (2010).
- [16] K. Baumann, R. Mottl, F. Brennecke, and T. Esslinger, Exploring Symmetry Breaking at the Dicke Quantum Phase Transition, Phys. Rev. Lett. 107, 140402 (2011).
- [17] F. Brennecke, R. Mottl, K. Baumann, R. Landig, T. Donner, and T. Esslinger, Real-time observation offluctuations at the drivendissipative Dicke phase transition, Proc. Natl. Acad. Sci. U.S.A. 110, 11763 (2013).
- [18] M. P. Baden, K. J. Arnold, A. L. Grimsmo, S. Parkins, and M. D. Barrett, Realization of the Dicke Model Using Cavity-

- Assisted Raman Transitions, Phys. Rev. Lett. 113, 020408 (2014).
- [19] X. Zhang, Y. Chen, Z. Wu, J. Wang, J. Fan, S. Deng, and H. Wu, Observation of a superradiant quantum phase transition in an intracavity degenerate Fermi gas, Science 373, 1359 (2021).
- [20] Z. Wu, J. Fan, X. Zhang, J. Qi, and H. Wu, Signatures of Prethermalization in a Quenched Cavity-Mediated Long-Range Interacting Fermi Gas, Phys. Rev. Lett. 131, 243401 (2023).
- [21] M. Feng, Y. P. Zhong, T. Liu, L. L. Yan, W. L. Yang, J. Twamley, and H. Wang, Exploring the quantum critical behavior in a driven Tavis-Cummings circuit, Nat. Commun. 6, 7111 (2015).
- [22] R. H. Zheng, W. Ning, Y. H. Chen, J. H. Lü, L. T. Shen, K. Xu, Y. R. Zhang, D. Xu, H. Li, Y. Xia, F. Wu, Z. B. Yang, A. Miranowicz, N. Lambert, D. Zheng, H. Fan, F. Nori, and S. B. Zheng, Observation of a Superradiant Phase Transition with Emergent Cat States, Phys. Rev. Lett. 131, 113601 (2023).
- [23] W. Ning, R. H. Zheng, J. H. Lü, F. Wu, Z. B. Yang, and S. B. Zheng, Experimental observation of spontaneous symmetry breaking in a quantum phase transition, Sci. China-Phys. Mech. Astron. 67, 220312 (2024).
- [24] M. L. Cai, Z. D. Liu, W. D. Zhao, Y. K. Wu, Q. X. Mei, Y. Jiang, L. He, X. Zhang, Z. C. Zhou, and L. M. Duan, Observation of a quantum phase transition in the quantum Rabi model with a single trapped ion, Nat. Commun. 12, 1126 (2021).
- [25] X. Zhao, Q. Bin, W. Hou, Y. Li, Y. Li, Y. Lin, X. Y. Lü, and J. Du, Experimental Observation of Parity-Symmetry-Protected Phenomena in the Quantum Rabi Model with a Trapped Ion, Phys. Rev. Lett. 134, 193604 (2025).
- [26] X. Chen, Z. Wu, M. Jiang, X. Y. Lü, X. Peng, and J. Du, Experimental quantum simulation of superradiant phase transition beyond no-go theorem via antisqueezing, Nat. Commun. 12, 6281 (2021).
- [27] Z. Wu, C. Hu, T. Wang, Y. Chen, Y. Li, L. Zhao, X. Y. Lü, and X. Peng, Experimental Quantum Simulation of Multicriticality in Closed and Open Rabi Model, Phys. Rev. Lett. 133, 173602 (2024).
- [28] M. Fruchart, R. Hanai, P. B. Littlewood, and V. Vitelli, Non-reciprocal phase transitions, Nature 592, 363 (2021).
- [29] S. Barzanjeh, M. Aquilina, and A. Xuereb, Manipulating the Flow of Thermal Noise in Quantum Devices, Phys. Rev. Lett. 120, 060601 (2018).
- [30] R. Huang, A. Miranowicz, J. Q. Liao, F. Nori, and H. Jing, Nonreciprocal Photon Blockade, Phys. Rev. Lett. 121, 153601 (2018)
- [31] A. Metelmann and A. A. Clerk, Nonreciprocal Photon Transmission and Amplification Via Reservoir Engineering, Phys. Rev. X 5, 021025 (2015).
- [32] D. Malz, L. D. Tóth, N. R. Bernier, A. K. Feofanov, T. J. Kippenberg, and A. Nunnenkamp, Quantum-Limited Directional Amplifiers with Optomechanics, Phys. Rev. Lett. 120, 023601 (2018).

- [33] Z. Shen, Y. L. Zhang, Y. Chen, F. W. Sun, X. B. Zou, G. C. Guo, C. L. Zou, and C. H. Dong, Reconfigurable optomechanical circulator and directional amplifier, Nat. Commun. 9, 1797 (2018).
- [34] Y. Wang, W. Xiong, Z. Xu, G. Q. Zhang, and J. Q. You, Dissipation-induced nonreciprocal magnon blockade in a magnon-based hybrid system, Sci. China-Phys. Mech. Astron. 65, 260314 (2022).
- [35] E. I. R. Chiacchio, A. Nunnenkamp, and M. Brunelli, Nonreciprocal Dicke Model, Phys. Rev. Lett. 131, 113602 (2023).
- [36] G. L. Zhu, C. S. Hu, H. Wang, W. Qin, X. Y. Lü, and F. Nori, Nonreciprocal Superradiant Phase Transitions and Multicriticality in a Cavity QED System, Phys. Rev. Lett. 132, 193602 (2024).
- [37] Y. J. Xu, L. H. Zhai, P. Fu, S. J. Cheng, and G. Q. Zhang, Non-reciprocal quantum phase transition in cavity magnonics, Phys. Rev. A 110, 043704 (2024)
- [38] Ö. O. Soykal and M. E. Flatté, Strong Field Interactions between a Nanomagnet and a Photonic Cavity, Phys. Rev. Lett. 104, 077202 (2010).
- [39] H. Huebl, C. W. Zollitsch, J. Lotze, F. Hocke, M. Greifenstein, A. Marx, R. Gross, and S. T. B. Goennenwein, High Cooperativity in Coupled Microwave Resonator Ferrimagnetic Insulator Hybrids, Phys. Rev. Lett. 111, 127003 (2013).
- [40] Y. Tabuchi, S. Ishino, T. Ishikawa, R. Yamazaki, K. Usami, and Y. Nakamura, Hybridizing Ferromagnetic Magnons and Microwave Photons in the Quantum Limit, Phys. Rev. Lett. 113, 083603 (2014).
- [41] X. Zhang, C. L. Zou, L. Jiang, and H. X. Tang, Strongly Coupled Magnons and Cavity Microwave Photons, Phys. Rev. Lett. 113, 156401 (2014).
- [42] M. Goryachev, W. G. Farr, D. L. Creedon, Y. Fan, M. Kostylev, and M. E. Tobar, High-Cooperativity Cavity QED with Magnons at Microwave Frequencies, Phys. Rev. Appl. 2, 054002 (2014).
- [43] D. Zhang, X. M. Wang, T. F. Li, X. Q. Luo, W. Wu, F. Nori, and J. Q. You, Cavity quantum electrodynamics with ferromagnetic magnons in a small yttrium-iron-garnet sphere, npj Quantum Inf. 1, 15014 (2015).
- [44] X. Zhang, C. L. Zou, N. Zhu, F. Marquardt, L. Jiang, and H. X. Tang, Magnon dark modes and gradient memory, Nat. Commun. 6, 8914 (2015).
- [45] L. Bai, M. Harder, Y. P. Chen, X. Fan, J. Q. Xiao, and C. M. Hu, Spin Pumping in Electrodynamically Coupled Magnon-Photon Systems, Phys. Rev. Lett. 114, 227201 (2015).
- [46] D. Lachance-Quirion, Y. Tabuchi, A. Gloppe, K. Usami, and Y. Nakamura, Hybrid quantum systems based on magnonics, Appl. Phys. Express 12, 070101 (2019).
- [47] B. Z. Rameshti, S. V. Kusminskiy, J. A. Haigh, K. Usami, D. Lachance-Quirion, Y. Nakamura, C. M. Hu, H. X. Tang, G. E. W. Bauer, and Y. M. Blanter, Cavity magnonics, Phys. Rep. 979, 1 (2022).
- [48] H. Y. Yuan, Y. Cao, A. Kamra, R. A. Duine, and P. Yan, Quantum magnonics: When magnon spintronics meets quantum information science, Phys. Rep. 965, 1 (2022).
- [49] Y. P. Wang, G. Q. Zhang, D. Zhang, X. Q. Luo, W. Xiong, S. P. Wang, T. F. Li, C. M. Hu, and J. Q. You, Magnon Kerr effect in a strongly coupled cavity-magnon system, Phys. Rev. B 94, 224410 (2016).
- [50] Y. P. Wang, G. Q. Zhang, D. Zhang, T. F. Li, C. M. Hu, and J. Q. You, Bistability of Cavity Magnon Polaritons, Phys. Rev. Lett. 120, 057202 (2018).

- [51] G. Q. Zhang, Y. P. Wang, and J. Q. You, Theory of the magnon Kerr effect in cavity magnonics, Sci. China-Phys. Mech. Astron. 62, 987511 (2019).
- [52] J. M. P. Nair, Z. Zhang, M. O. Scully, and G. S. Agarwal, Nonlinear spin currents, Phys. Rev. B 102, 104415 (2020).
- [53] M. X. Bi, X. H. Yan, Y. Zhang, and Y. Xiao, Tristability of cavity magnon polaritons, Phys. Rev. B 103, 104411 (2021).
- [54] R. C. Shen, Y. P. Wang, J. Li, S. Y. Zhu, G. S. Agarwal, and J. Q. You, Long-Time Memory and Ternary Logic Gate Using a Multistable Cavity Magnonic System, Phys. Rev. Lett. 127, 183202 (2021).
- [55] R. C. Shen, J. Li, Z. Y. Fan, Y. P. Wang, and J. Q. You, Mechanical Bistability in Kerr-modified Cavity Magnomechanics, Phys. Rev. Lett. 129, 123601 (2022).
- [56] Z. Zhang, M. O. Scully, and G. S. Agarwal, Quantum entanglement between two magnon modes via Kerr nonlinearity driven far from equilibrium, Phys. Rev. Res. 1, 023021 (2019).
- [57] Z. B. Yang, H. Jin, J. W. Jin, J. Y. Liu, H. Y. Liu, and R. C. Yang, Bistability of squeezing and entanglement in cavity magnonics, Phys. Rev. Res. 3, 023126 (2021).
- [58] W. Xiong, M. Tian, G. Q. Zhang, and J. Q. You, Strong longrange spin-spin coupling via a Kerr magnon interface, Phys. Rev. B 105, 245310 (2022).
- [59] C. Kong, H. Xiong, and Y. Wu, Magnon-Induced Nonreciprocity Based on the Magnon Kerr Effect, Phys. Rev. Applied 12, 034001 (2019).
- [60] M. Ullah and S. Mikki, Nonreciprocal microwave field transmission in a quantum magnomechanical system controlled by magnetostriction and Kerr nonlinearities, Phys. Rev. B 109, 214303 (2024).
- [61] Q. Miao and G. S. Agarwal, Kerr nonlinearity induced nonreciprocity in dissipatively coupled resonators, Phys. Rev. Research 6, 033020 (2024).
- [62] J. Chen, X. G. Fan, W. Xiong, D. Wang, and L. Ye, Nonreciprocal entanglement in cavity-magnon optomechanics, Phys. Rev. B 108, 024105 (2023).
- [63] J. Chen, X. G. Fan, W. Xiong, D. Wang, and L. Ye, Nonreciprocal photon-phonon entanglement in Kerr-modified spinning cavity magnomechanics, Phys. Rev. A 109, 043512 (2024).
- [64] R. Ahmed, H. Ali, A. Shehzad, S. K. Singh, A. Sohail, and M. C. de Oliveira, Nonreciprocal Multipartite Entanglement in a two-cavity magnomechanical system, arXiv:2405.16221v2.
- [65] D. Kong, J. Xu, and F. Wang, Nonreciprocal entanglement of ferrimagnetic magnons and nitrogen-vacancy-center ensembles by Kerr nonlinearity, Phys. Rev. Applied 21, 034061 (2024).
- [66] D. Kong and F. Wang, Nonreciprocal steering between optical and microwave waves by Bogoliubov cooling in a cavity optomagnonic system, Phys. Rev. A 111, 013704 (2025).
- [67] H. Q. Zhang, S. S. Chu, J. S. Zhang, W. X. Zhong, and G. L. Cheng, Nonreciprocal magnon blockade based on nonlinear effects, Opt. Lett. 49, 2009 (2024).
- [68] J. L. Tong, Y. Hao, S. X. Wu, C. H. Bai, and S. Bai, Nonreciprocal Strong Mechanical Squeezing Based on the Kerr Effect in Cavity-Magnon Optomechanical System, Adv. Quantum Technol. 8, 2400654 (2025).
- [69] D. F. Walls and G. J. Milburn, Quantum Optics (Springer, Berlin, 1994).
- [70] I. S. Gradshteyn and I. M. Ryzhik, *Table of Integrals, Series and Products* (Academic Press, Orlando, 1980).
- [71] C. J. Zhu, L. L. Ping, Y. P. Yang, and G. S. Agarwal, Squeezed light induced symmetry breaking superradiant phase transition, Phys. Rev. Lett. 124, 073602 (2020).